International Journal of GEOMATE, May 2023, Vol. 24, Issue 105, pp.85-92
ISSN: 2186-2982 (P), 2186-2990 (O), Japan, DOI: https://doi.org/10.21660/2023.105.s8561
Geotechnique, Construction Materials and Environment

STRESS ANALYSIS OF VALLEY FILLS CONSIDERING RAINFALL INFILTRATION CONDITIONS

Daiki Yamashita[1] and *Shin-ichi Kanazawa[2]

[1]Environmental Science and Technology, Master's Program Graduate School of Science and Technology Niigata University, Japan;[2] Civil Engineering Program, Faculty of Engineering, Niigata University, Japan

*Corresponding Author, Received:15 March 2022, Revised: 01 Feb. 2023, Accepted: 12 March 2023

ABSTRACT: In recent years, many cases of collapse and damage of soil structures have been reported worldwide due to the sudden increase in heavy rainfall due to climate change. However, analysis of the factors that lead to the fracture of these structure and the fracture mechanisms have not been fully investigated. Therefore, numerical analysis is attracting attention as a way to better understand the behavior of ground under various construction and rainfall conditions to ensure the ultra-long-term safety of soil structures and to extend their life. Under these circumstances, we performed in this study a construction analysis of valley fills by using three types of materials (sand, silt-mixed sand, and sand-mixed silt) and rainfall analysis under multiple conditions and intensities. From the analysis results, we conclude that the weakening of valley fills can be roughly divided into three patterns according to the relationship between the flow rate due to rainfall and the infiltration rate of the embankment material.

Keywords: Valley fills, Finite element analysis, Rainfall analysis

1. INTRODUCTION

In recent years, many cases of collapse and damage to soil structures have been reported due to the increase in sudden heavy rains due to climate change, such as guerrilla rainstorms and typhoons. The danger of sediment-related disasters increasingly plague us every year. Even in the last few years, major disasters are still fresh in our memory, such as the flooding and collapse of river embankments caused by the typhoon in East Japan in the first year of Reiwa and the landslide that occurred in Izusan district, Atami City, Shizuoka Prefecture, in the third year of Reiwa. In addition, the typhoon in East Japan in the first year of Reiwa broke 140 embankments nationwide. These disasters are becoming a familiar problem in our daily lives. Therefore, it is necessary to suppress the collapse of soil structures, and countermeasures for that are required.

Factors that cause the embankment structure to fail include the foundation ground, embankment material, degree of compaction during construction, and water drainage treatment. In particular, water drainage treatment is often the cause of destruction. However, the factor analysis and the mechanism of how the actual embankment structure leads to failure are not sufficiently clarified at present. Here, the soil consists of three phases, a solid phase, a liquid phase, and an air phase, and it often exists in an unsaturated state containing air and dissolved air in the embankment and the foundation ground below the groundwater table. As a result, pore air is dissolved or released into the liquid phase by permeation of rainfall, and the soil appears to be volume-compressed. However, it cannot be said that such an unsaturated state is sufficiently considered in the current guidelines, and it is considered that sufficient drainage measures cannot be provided.

Focusing on the embankment construction method, it can be roughly divided into specification design and performance design. Here, the specification design defines the conditions at the time of construction uniformly, and the design itself does not specify the service life. Therefore, in recent years, there has been a shift to performance design that guarantees that the required performance is satisfied throughout the service life of the design, and numerical analysis is expected as a method of examining required performance.

From the above points, it is an urgent need to predict the stress behavior of the embankment considering the unsaturated state using numerical analysis. In previous studies, stress analysis was carried out from the initial stage of embankment construction considering the unsaturated state, and long-term stress analysis was performed to clarify the characteristics of the stress inside the embankment depending on the construction conditions and construction period [1] [2] [3]. On the other hand, it is known that various embankment materials are used depending on the site and situation, but there are few studies that show the stress behavior and rainfall infiltration characteristics of each embankment material considering the unsaturated state. Therefore, the details have not been clarified.

Against this background, this study will analyze the construction of valley-filled embankment using three types of materials (sand, silt-mixed sand, and sand-mixed silt) and rainfall analysis under multiple conditions and intensities. Based on the results, we aimed to analytically examine changes in ground behavior when materials and rainfall conditions were changed.

2. RESEARCH SIGNIFICANCE

Through this study, by clarifying the infiltration characteristics of rainfall and the weakening process of embankments for each embankment material and rainfall intensity, it is thought that it will be possible to easily pick up embankments that have problems with wastewater treatment among many embankments. This is expected to bring about effects such as making it possible to quickly take measures against actual embankments. In addition, since it is possible to pick up countermeasure embankments based on the analysis results, the amount of work at the site will be reduced, and we believe that it will be possible to throw a stone at the problem of the shortage of construction workers in Japan.

3. AIR-DISSOLVED UNSATURATED SOIL / WATER / AIR COUPLED FINITE ANALYSIS

In this study, we use the air-dissolved unsaturated soil / water / air coupled finite analysis code “DACSAR-MP” [4]. The unsaturated soil elasto-plastic composition model, water retention curve model, and finite element formulation in this analysis code are as shown below.

3.1 The Unsaturated Soil Elasto-plastic Composition Model

So far, several unsaturated soil composition models have been proposed, but the elasto-plastic composition model of unsaturated soil proposed by Ohno et al. [5] is used in this analysis code. Ohno et al. [5] propose a model in which the effective saturation is used as a state agent to express the rigidity, with reference to the model given the definition of effective stress considering the water content of Karube et al. [6]. The effective stress is given by the following equations, Equation (1) shows the effective stress, Equation (2) shows the basic stress tensor and attractive stress, and Equation (3) shows the attractive force.

$$\boldsymbol{\sigma}' = \boldsymbol{\sigma}^N + p_s\mathbf{1} \tag{1}$$

$$\boldsymbol{\sigma}^N = \boldsymbol{\sigma} - p_a\mathbf{1},\ \ p_s = sS_e \tag{2}$$

$$s = p_a - p_w,\ \ S_e = \frac{S_r - S_{rc}}{1 - S_{rc}} \tag{3}$$

Here, $\boldsymbol{\sigma}'$ is the effective stress tensor; $\boldsymbol{\sigma}^N$ is the base stress tensor; $\boldsymbol{\sigma}$ is the total stress tensor; $\mathbf{1}$ is the second order unit tensor; p_a is the pore air pressure; p_s is the suction stress; s is the suction; p_w is the pore water pressure; S_e is the effective degree of saturation; and S_{rc} is the degree of saturation at $s \to \infty$.

Furthermore, in this study, the EC model of Ohno et al. [7], who has no singular point (Ex: Pre-consolidation stress at saturation) on the yield surface, was incorporated into the analysis code in order to avoid shifting to a singular point that cannot be differentiated in numerical calculation. The EC model is an elasto-plastic composition model that expresses the soil's contractility characteristics as an exponential function, and Ohno et al. [7] derived the yield function of unsaturated soil as follows.

$$f\left(\boldsymbol{\sigma}', \zeta, \varepsilon_v^p\right) = MD\ln\frac{p'}{\zeta p'_{sat}} + \frac{MD}{n_E}\left(\frac{q}{Mp'}\right)^{n_E} - \varepsilon_v^p = 0 \tag{4}$$

Here, p'_{sat} is the yield stress at saturation; p' is mean effective principal stress; q is axial stress; M is the q/p' in the limit state; D is the dilatancy coefficient; ε_v^p is the plastic volume strain; and n_E is the shape parameter.

In addition, the increase in consolidation yield stress due to desaturation is expressed in the form of ζ times the consolidation yield stress p'_{sat} in the saturated state. ζ is a function of the effective saturation and can be expressed as the following equation.

$$\zeta = \exp\left[(1 - S_e)^b \ln a\right] \tag{5}$$

Here, b is parameter to adjust the spacing of the isosaturation lines on plane $e - \ln p'$; a is parameter that determines the multiplication factor of the consolidation yield stress when the increase in rigidity due to desaturation is maximum. In particular, a is often treated as a fitting parameter.

Substituting $n_E = 1.0$ into Equation (4) gives the following equation.

$$f\left(\boldsymbol{\sigma}', \zeta, \varepsilon_v^p\right) = MD\ln\frac{p'}{\zeta p'_{sat}} + D\eta - \varepsilon_v^p = 0 \quad (\eta = \frac{q}{p'}) \tag{6}$$

From Equations (3) and (5), it is shown that Equation (6) is the original Cam-Clay model [8] because it is $\zeta = 1$ in the saturated state ($S_e = 1$).

Fig.1 shows a conceptual diagram of the yield surface of unsaturated soil shown by the S_e - Hardening model [5], and Fig.2 shows the yield surface of the EC model proposed by Ohno et al. [7]. This shows that the larger n_E is, the more the singular point is eliminated and it becomes differentiable, and

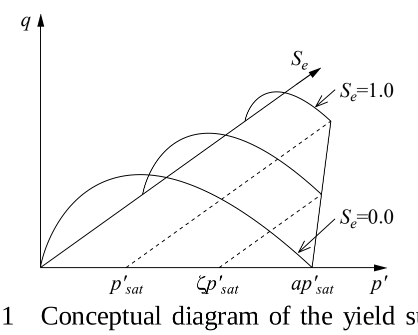

Fig. 1 Conceptual diagram of the yield surface of unsaturated soil

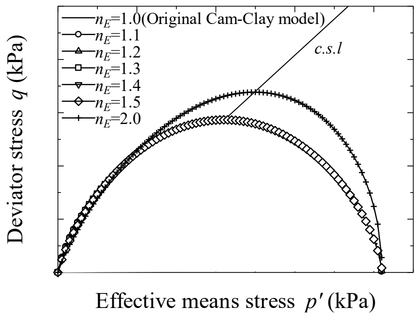

Fig. 2 Yield surface of EC model

in the case of $n_E = 2.0$, it is similar to the modified Cam-Clay model [9]. In this analysis code, it is used as an isotropic model.

3.2 Moisture Characteristic Curve Model

It is widely known that the water retention curve (suction-saturation relationship) that influences the mechanical behavior of unsaturated soil differs between dehydration and water absorption. In other words, the water characteristic curve showing the suction-saturation relationship is not unique, and there are innumerable scanning curves depending on the water retention state during dehydration or water absorption. Therefore, Kawai et al. [10] proposed a water characteristic curve model capable of expressing hysteresis by utilizing the fact that these scanning curves have similar shapes during dehydration and water absorption. In addition to the model capable of hysteresis expression, this analysis code uses the logistic curve equation as shown in Fig.3. Here, the figure is "(1) dehydration curve" and "(2) water absorption curve" drawn on the dehydration side and the water absorption side from an arbitrary suction-saturation state, which was proposed by Sugii and Uno [11].

Here, the dehydration curve that passes through an arbitrary suction-saturation degree (s_1, S_{r1}) converges to the limit water content ratio w_C at $s \to \infty$, and if the influence of the gap is ignored, the saturation degree that converges at $s \to \infty$ is $S_{rc} = G_s w_c / e$. Here, G_s is soil particle specific density; e is void ratio. Using S_{rf}^* obtained in this way, the dehydration curve is expressed by the following equation.

$$S_r = \frac{S_{rf}^* - S_{rc}}{1 + \exp\left(A^D + B^D \log_e s_1\right)} + S_{rc} \tag{7}$$

Here, S_e is the effective degree of saturation; S_r is the degree of saturation; s is the suction; S_{rc} is the degree of saturation at $s \to \infty$; S_{rf} is the degree of saturation in $s = 0$; A, B are fitting parameters of moisture characteristics (subscript D indicates dehydration).

Next, the water absorption curve that passes through an arbitrary suction-saturation degree (s_1, S_{r1}) has a non-constant convergence saturation at $s \to \infty$, so unlike the dehydration curve, two parameters S_{ra} and S_{rf} must be determined. In other words, it is sufficient to find S_{ra}^* that satisfies the following equation.

$$\frac{S_{r1} - S_{ra}}{S_{rf}\left(S_{ra}^*\right) - S_{ra}^*} = \frac{1}{1 + \exp\left(A^W + B^W \log_e s_1\right)} \tag{8}$$

As a result, the dehydration curve and water absorption curve at any suction-saturation degree can be obtained. Here, the subscript W indicates the water absorption.

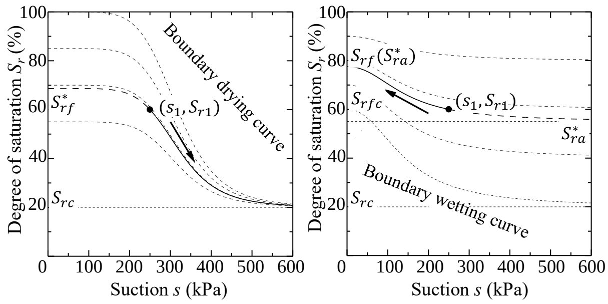

(1) Dehydration curve (2) Water absorption curve

Fig. 3 Moisture characteristic curve model

3.3 Finite Element Formulation

The governing equation in the unsaturated soil / water / air coupled problem consists of balanced ceremony, effective stress formula, unsaturated elasto-plastic constitutive equation, conformity expression, Darcy's rule, air Darcy's rule, continuous conditional expression, and continuous conditional expression considering gas phase, and is given by the following equations.

・Balanced ceremony

$$\mathrm{div}\boldsymbol{\sigma}^T + \rho\mathbf{g} = 0, \quad \boldsymbol{\sigma} = \boldsymbol{\sigma}^T \tag{9}$$

・Effective stress formula

$$\boldsymbol{\sigma}' = \boldsymbol{\sigma}^N + p_S\mathbf{1}, \quad \boldsymbol{\sigma}^N = \boldsymbol{\sigma} - p_a\mathbf{1} \tag{10}$$

・Unsaturated elasto-plastic constitutive equation

$$\dot{\boldsymbol{\sigma}}' = \mathbf{D} : \dot{\boldsymbol{\varepsilon}} - \mathbf{C}^S \dot{S}_e \tag{11}$$

・Conformity expression

$$\boldsymbol{\varepsilon} = -\frac{1}{2}\left(\nabla\mathbf{u}\right)^S \tag{12}$$

・Darcy's rule

$$\tilde{\boldsymbol{v}} = -\mathbf{k} \cdot \mathrm{grad}h \tag{13}$$

・Air Darcy's rule

$$\tilde{\boldsymbol{v}}_a = -\mathbf{k}_a \cdot \mathrm{grad}p_a \tag{14}$$

・Continuous conditional expression

$$n\dot{S}_r - S_r\dot{\varepsilon}_v + \mathrm{div}\tilde{\boldsymbol{v}} = 0 \tag{15}$$

・Continuous conditional expression considering gas phase

$$(1-S_r)\dot{\varepsilon}_v + n\dot{S}_r - n(1-S_r)\frac{\dot{p}_a}{K_a} - \mathrm{div}\tilde{\mathbf{v}}_a = 0 \qquad (16)$$

Here, assuming that the saturation is a function that can be expressed only by suction, the following equation is obtained.

$$\dot{S}_r = \frac{dS_r}{ds}\dot{s} = -\frac{dS_r}{ds}\dot{p}_W \qquad (17)$$

In addition, the increment of suction stress in Equation (10) is calculated by the following equation.

$$\begin{aligned}\dot{p}_S &= \frac{\dot{S}_r}{1-S_{rc}}s + \frac{S_r - S_{rc}}{1-S_{rc}}\dot{s} \\ &= \frac{1}{1-S_{rc}}\left(\frac{dS_r}{ds}s + S_r - S_{rc}\right)\dot{s}\end{aligned} \qquad (18)$$

However, S_{rc} is considered to be the saturation degree indicated by the adsorbed aqueous phase, and is a material constant.

Here, $\boldsymbol{\sigma}'$ is the effective stress tensor; $\boldsymbol{\sigma}^N$ is the base stress tensor; $\boldsymbol{\sigma}$ is the total stress tensor; p_s is the suction stress; p_a is the pore air pressure; $\mathbf{D}$ is the elastic stiffness tensor; $\boldsymbol{\varepsilon}$ is the strain tensor; $\mathbf{C}^S$ is the coefficient tensor; S_e is the effective degree of saturation; $\mathbf{u}$ is the displacement vector; $\tilde{\mathbf{v}}$ is the flow velocity vector of interstitial water; $\mathbf{k}$ is the permeability coefficient tensor; h is the all head; S_r is the degree of saturation; ε_v is the volumetric strain; n is the porosity; K_a is the air pressure; $\tilde{\mathbf{v}}_a$ is the flow velocity vector of interstitial air; and the superscript s indicates the symmetric part of the tensor in ( ).

By weakly formalizing the above governing equation, discretizing it spatially and temporally, and solving it under the conditions of initial value and boundary value, the solutions of unknowns $\{\Delta\mathbf{u}^N\}$, $\{\Delta\mathbf{h}^N|_{t=t+\Delta t}\}$, and $\{\Delta\mathbf{p}_a^N|_{t=t+\Delta t}\}$ can be obtained.

Here, $\Delta\mathbf{u}^N$ is the amount of change in node displacement; $\Delta\mathbf{h}^N$ is the amount of change in total head in minute time Δt; $\Delta\mathbf{p}_a^N$ is the amount of change in air pressure in a minute time Δt.

4. ANALYSIS MODEL DETERMINATION AND CONSTRUCTION METHOD

4.1 About The Analysis Model

In this study, we perform construction-rainfall analysis for valley fills. There are various standards and formats for the valley fills, but in this study, the analysis model shown in Fig.4 is used as the finite analysis model. The size of the valley fills structure is a trapezoid with an upper side of 18m, a lower side of 10m, and a height of 3m. The foundation ground is set to surround the embankment, with a total length of 3.6m and width of 20m. The embankment is composed of a total of 400 meshes, 10 in the vertical direction and 40 in the horizontal direction. The displacement boundary, head boundary, and air boundary are shown in Fig. 4.

In addition, the road earthwork-embankment guideline [12] states that the embankment material should be easy to use in construction, maintain the safety of the embankment, and not cause harmful deformation. With this guideline, structures are constructed using a wide range of materials, as shown in Table 1. Therefore, in this study, we will perform construction-rainfall analysis considering three types of materials that imitate "sand", "sand-mixed silt", and "silt-mixed sand". Each material parameter and moisture characteristic curve are shown in Table 1 and Fig.5. These parameters were determined with reference to the research results by Honda, Iizuka, Ohno, Kawai and Wang [13]. The parameters shown below are for use in the embankment. When these materials are used for the foundation, the

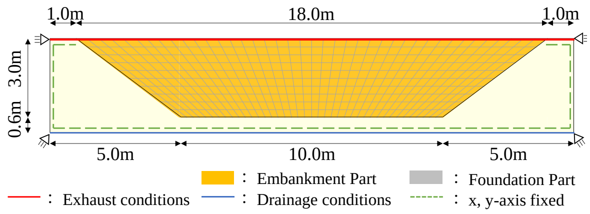

Fig. 4 Finite element analysis model

Table 1 Material parameters

M	m	n
1.33	0.80	1.0
n_E	e_0	ν
1.3	1.2	0.33
S_{r0}	S_{r-0}	G_s
0.15	0.50	2.7

Common to all materials

λ		
Sand	Silt-sand	Sand-silt
0.10	0.12	0.18
κ		
Sand	Silt-sand	Sand-silt
0.010	0.012	0.018
k_x, k_y [m/day]		
Sand	Silt-sand	Sand-silt
8.7	0.87	0.087

Different materials

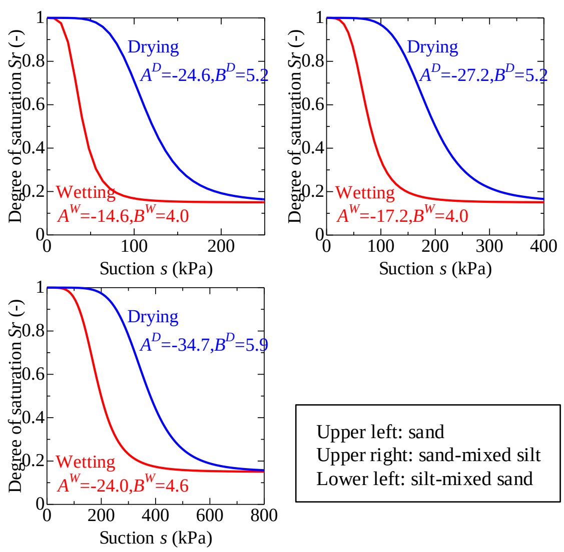

Fig. 5 Moisture characteristic curve

permeability coefficient was lowered by 2 orders to make the foundation less permeable than the embankment portion of the model.

Regarding the material parameters, λ is the expansion index; κ is the compression index; M is the limit state parameter; m is the unsaturated permeability coefficient of Mualem [14]; n is the E_c model parameter; n_E is the enlargement ratio of yield surface; e_0 is the initial void ratio; ν is the Poisson's ratio; k_x is the permeability coefficient in the x-axis direction [m/day]; k_y is the permeability coefficient in the y-axis direction [m/day]; S_{r0} is the critical saturation; and G_s is the soil particle density.

4.2 Construction Analysis

4.2.1 Construction method

In this study, after performing the construction analysis of the valley fills under the above-mentioned conditions, the rainfall analysis was performed by giving the upper surface of the embankment a flow rate similar to rainfall. However, there are few existing examples of numerical analysis of valley fills by construction method. Therefore, the construction analysis was performed by each of the following four construction methods, and the construction method to use for the analysis was determined from the results.

The construction method is as follows.

① The foundation and embankment portions of the structure are generated all at once.
② After generating the foundation, the embankment is generated all at once.
③ After generating the foundation, the embankment is divided into 10 layers for every 30cm of layer thickness.
④ After generating the foundation, the embankment is generated with a layer thickness of 30cm compacted with 300kPa (repeated for a total of 10 layers).

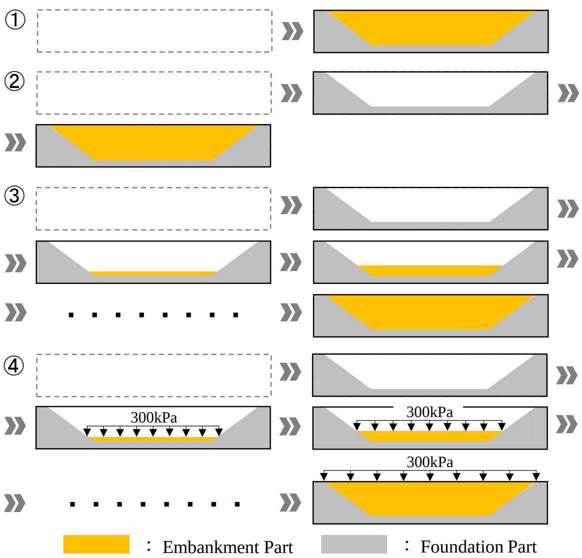

Fig. 6 How to construct valley fills

After the construction was complete, a flow rate equivalent to a rainfall intensity of 100mm/hour was given to the upper surface of the embankment until the total flow rate reached 200mm. The ground behavior of each case was compared. In this investigation, the analysis model and various boundary conditions are as described in the previous section, and the material used is "sand".

4.2.2 Construction analysis results

Fig.7 shows the analysis results of the various construction methods described in the previous section. The results show only the left half of the model is shown.

From the above analysis results, effective mean stress p', degree of saturation S_r, void ratio e, shear strain ε_s, and suction s demonstrate the following tendencies in all construction methods, and no significant difference in ground behavior depending on the construction method was observed.

・Effective mean stress p'

Stress decreases in the upper part of the embankment and near the boundary between the embankment and the foundation.

・Degree of saturation S_r

Degree of saturation increases near the upper surface of the embankment.

・Shear strain ε_s

Shear strain occurs along the boundary between the embankment and the foundation.

・Suction s

Suction disappears near the upper surface of the embankment.

For the void ratio e, the results show a decrease at the boundary between the embankment and the foundation for all construction methods. However, in the construction methods ③ and ④, in which the embankment is divided into layers, the range in which

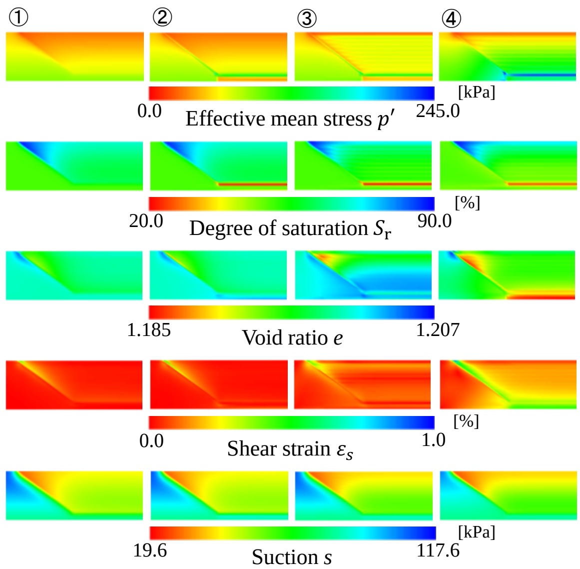

Fig. 7 Construction analysis results

the void ratio decreases is wide. Furthermore, in construction method ③, an increase in the void ratio between the bottom of the embankment and the foundation also occurs. This was contrary to what was expected from the results of change in saturation, as it is uncommon for the porosity ratio at the bottom of the embankment to rise, that is, for the volume to expand before rainfall has penetrated to the bottom.

Based on the above results, construction method①, where “the foundation and embankment are generated all at once", was adopted for this study.

5. CONSTRUCTION / RAINFALL ANALYSIS CONSIDERING VARIOUS MATERIALS

5.1 Construction / Rainfall Analysis Conditions

To clarify the changes to the in-ground behavior of the valley fills by material type and rainfall intensity, construction and rainfall analysis were performed in this study using the combinations shown in Table 2. The analysis model and construction method used were as described in the previous section. In addition, for rainfall analysis, rainfall was applied only to the upper surface of the embankment after the valley fills was constructed. Regarding the rainfall intensity, two patterns were applied: 10mm/hour, which is defined as slightly heavy rain, and 100mm/hour, which is defined as heavy rain.

Furthermore, in order to investigate how the behavior of the ground changes due to actual heavy rainfall, rainfall analysis was performed with reference to the rainfall data of the East Japan Typhoon in the first year of Reiwa [15].

Table 2 Analysis pattern

	100mm/hour	10mm/hour	2019 Typhoon No.19
Sand	Pattern 1	Pattern 4	Pattern 7
Silt-mixed sand	Pattern 2	Pattern 5	-
Sand-mixed silt	Pattern 3	Pattern 6	-

Embankment material   Rainfall

5.2 Construction / Rainfall Analysis Results

5.2.1 Analysis results focusing on materials

Fig. 8 shows the results of construction and rainfall analysis of various materials at a rainfall intensity of 10mm/hour. The results show only the left half of the model is shown. The duration of rainfall was 20 hours, and the total rainfall was 200mm.

First, we examine effective mean stress p' and compare each stress distribution. The results confirmed that the more permeable the material, the lower the effective mean stress across a wide area of the embankment. This is thought to be due to the disappearance of suction and the increase in pore water pressure due to rainfall. It was also confirmed that the stress value near the boundary between the embankment and the foundation decreased regardless of material.

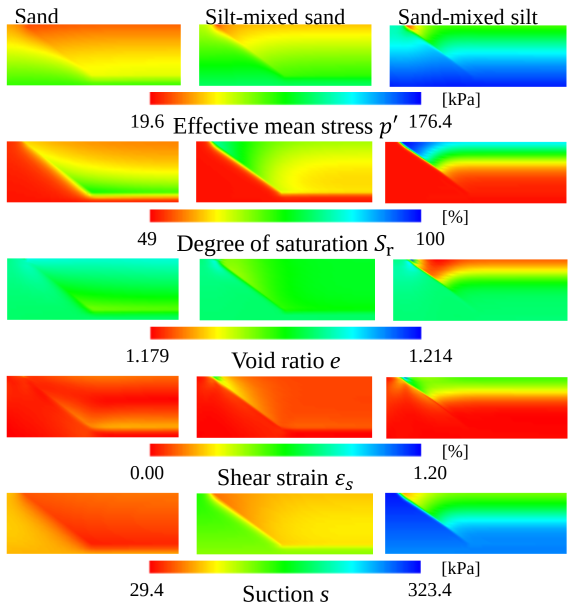

Fig. 8 Analysis results focusing on materials

Next, we examine degree of saturation S_r and compare each distribution. The results confirm that the poorer the permeability of the material, the more the saturation inside the embankment progresses. In addition, the more impervious the material, the more rainfall permeates the upper surface of the embankment. Therefore, impervious material cannot allow rainfall to penetrate the inside of the embankment. On the other hand, these results confirmed that rainfall penetrated to the bottom of the embankment with materials having good permeability, such as sand, and the characteristics of rainfall penetration for each embankment material could be reproduced.

Finally, we compare each distribution of shear strain ε_s. These results confirmed that, as with the distribution of the degree of saturation, larger shear strain occurred in materials with poorer permeability. Examining the location of shear strain reveals that a large value was generated where saturation had progressed into all the embankment material. However, the maximum shear strain in this analysis was about 1.20%, suggesting that the embankment was weakened, but likely not to the point leading to fracture.

The above results confirm that when focusing on material type, materials with poor permeability promote saturation on the upper surface of the embankment and structures built with these materials may weaken with rainfall.

5.2.2 Analysis results focusing on rainfall intensity

Fig. 9 shows the analysis results of construction method by each rainfall intensity in the material "sand". Only the left half of the model is shown in the figure. The duration of rainfall was 2 hours at a rainfall intensity of 100m/hour and 20 hours at a rainfall intensity of 10mm/hour. The total rainfall was

200mm.

First, we examine effective mean stress p' and compare both stress distributions. The results confirm that the stress value decreased as rainfall intensity increased. As mentioned above, this is thought to be due to the disappearance of suction and the increase in pore water pressure due to rainfall.

Next, we look at the degree of saturation S_r and compare both distributions. These results confirm that saturation progresses as rainfall intensity increases. In addition, saturation progresses only to the top edge of the embankment at a rainfall intensity of 100mm/hour; whereas, saturation progresses to the bottom of the embankment at a rainfall intensity of 10mm/hour. It is probable that rapid rainfall with a rainfall intensity of 100mm/hour did not allow the rainfall to penetrate into the embankment. On the other hand, at a rainfall intensity of 10mm/hour, there was sufficient margin for rainfall penetration, so rainfall likely penetrated to the bottom of the embankment and saturation progressed.

Finally, we compare both distributions of shear strain ε_s. The shear strain results confirm that there was no large difference in the shear strain values between the two rainfall intensities, but there was a large difference in the location of where the shear strain occurred. Similar to the above discussion of saturation, the shear strain values tended to increase at the areas where saturation progressed. Shear strain was confirmed near the boundary between the embankment and the foundation at a rainfall intensity of 100mm/hour, and at the bottom of the embankment at a rainfall intensity of 10mm/hour. Here, the maximum value of shear strain was about 0.4%. As mentioned above, this does not lead to the destruction of the embankment, but it does suggest that progressive weakening may occur at the affected sites.

The above analysis results confirm that the area of valley fills weakening differs depending on the difference in rainfall intensity.

5.2.3 Rainfall analysis results simulating full-scale heavy rainfall

In this study, rainfall analysis using actual heavy rainfall data was carried out, and changes in ground behavior over time were also be investigated. In this analysis, we analyzed the rainfall with reference to the rainfall data from the typhoon in East Japan in the first year of Reiwa. The data used is the maximum 24-hour rainfall during the East Japan typhoon in the first year of Reiwa at the meteorological observation point in Mitsumine, Chichibu City, Saitama Prefecture. The total rainfall is 561.5mm/hour.

Fig. 11 shows the time course of each parameter for the study elements of the embankment in the rainfall analysis. The study elements are as described in Fig.10. As a general feature, analysis results confirmed that the effective mean stress decreased, the degree of saturation increased, the void ratio decreased, shear strain was present, and suction disappeared in the entire embankment. This indicates that the stress decreases with volume compression, and, considering the $e - \ln p'$ relation, it demonstrated that there is a tendency for weakening throughout the embankment. This was particularly remarkable in A, an element at the bottom of the embankment. Furthermore, from around 10 hours, when the rainfall intensity became high, a remarkable increase in the degree of saturation and a decrease in the void ratio were confirmed in C, the upper surface element of the embankment. This suggests that there is a tendency for weakening near this element. Comparing the behaviors of the elements at the same depth (B-D, C-E) confirmed that the elements at the end of the embankment had a significant increase in the degree of saturation and a higher occurrence of shear strain compared to the elements at the center of the embankment.

The above suggests that as a result of the actual-scale heavy rainfall, the valley fills tend to weaken in the vicinity of the boundary between the embankment and the foundation.

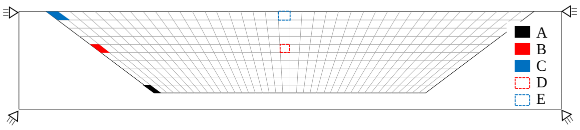

Fig. 10 The study elements

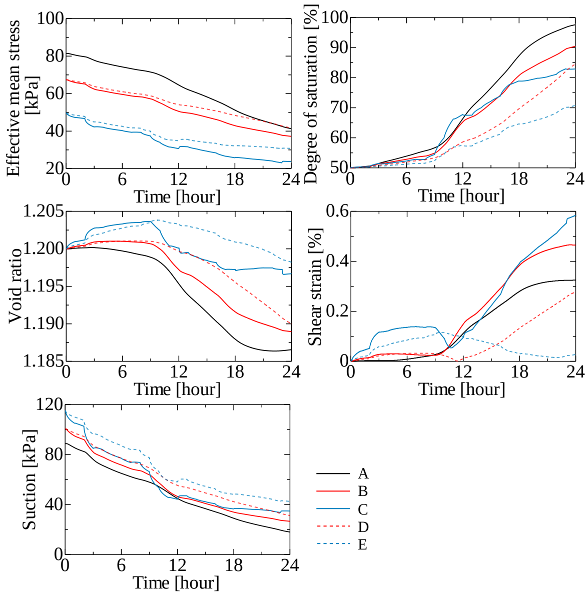

Fig. 11 Time course of each parameter

5.3 Discussion of Result

The analysis results suggested that the embankment weakened regardless of the soil material and rainfall intensity. However, it became clear that the tendency differs depending on the material and rainfall intensity, and the tendency of weakening can be roughly divided into the following three patterns based on the relationship between the permeability of the embankment material and the rainfall intensity.

(1) Rainfall > Permeability (Penetration rate)

Although rainfall permeates the lower layer, not all rainfall permeates, and it becomes saturated from the upper layer, which tends to weaken accordingly.

(2) Rainfall < Permeability (Penetration rate)

The valley fills become saturated from the lower layer (bottom) of the embankment and tends to weaken accordingly.

(3) Rainfall ≪ Permeability (Penetration rate)

Only the upper layer tends to saturate without penetrating from the upper layer to the lower layer of the embankment. At this time, rapid saturation leads to destruction of the structure.

In addition, it was clarified that rainfall infiltration proceeds along the boundary between the foundation and the embankment in all cases.

6. CONCLUSION

In this study, we clarified the stress behavior and rainfall infiltration characteristics in the unsaturated state by conducting construction and rainfall analysis of the valley fills focusing on the material and rainfall conditions using unsaturated soil/water/air coupled finite element analysis. From the results of each analysis, it was clarified that the places and tendencies of weakening and destruction differed depending on the embankment material and rainfall intensity, and it was concluded that the permeability of the embankment material was greatly involved. From this, we could confirm the usefulness of evaluating the stress and rainfall infiltration characteristics of unsaturated soil using numerical analysis. However, the strength and deformation characteristics of the embankment change greatly depending on the rainfall history, etc., and the conclusions in this study are based on limited conditions. In the future, it will be necessary to conduct this analysis under conditions that are more suitable for the natural environment. In the future, we would like to conduct a more practical evaluation considering various situations by changing the material parameters and rainfall intensity.

7. REFERENCES

[1] Kanazawa S. and Suzuki S.: Stress analysis of embankment due to different in construction conditions, International Journal of GEOMATE, Vol.18, Issue 65, 2020, pp. 1 – 8.

[2] Nakamura E. and Kanazawa S.: Analytical study on quality evaluation of embankment structure with a view to longer life, International Journal of GEOMATE, Vol.20, Issue 78, 2021, pp.177-182.

[3] Kanazawa S. and Igarashi H.: Analysis of embankment stress produced during construction and in-service phases considering embankment geometries, International Journal of GEOMATE, Vol.20, Issue 79,2021, pp.68-73.

[4] Kanazawa S., Toyoshima K., Kawai K., Tachibana S. and Iizuka A.: Analysis of mechanical behavior of compacted soil with F.E. method, journal of JSCE, No.68 (2), 2012 , pp.291-298.

[5] Ohno S., Kawai K. and Tachibana S.: Elasto-plastic constitutive model for unsaturated soil applied effective degree of saturation as a parameter expressing stiffness, journal of JSCE, Vol.63/No.4, 2007, pp.1132-1141.

[6] Karube D., Kato S., Hamada K. and Honda M.: The relationship between the mechanical behavior and the state of porewater in unsaturated soil, journal of JSCE, No.535/III-34, 1996, pp.83-92.

[7] Ohno S., Iizuka A. and Ohta H.: Two categories of new constitutive model derived from non-linear description of soil contractancy, Journal of applied mechanics, 2006, pp. 407-414

[8] Schofield A. and Wroth P.: Critical State Soil Mechanics, McGraw-Hill, 1968, pp. 1-310.

[9] Roscoe, K. H and Burland, J. B.: On the Generalised Stress-Strain Behavior of Wet Clay, Engineering Plasticity eds. J. Heyman and F. A. Leckie, Cambridge University Press, 1968, pp.535-609.

[10] Kawai K., Wang W. and Iizuka A.: The expression of hysteresis appearing on water characteristic curves and the change of stresses in unsaturated soils, Journal of applied mechanics, Vol.5, 2002, pp.777-784.

[11] Sugii T. and Uno T.: Modeling the New Moisture Characteristic Curve, Journal of JSCE, 1995, pp.130-131.

[12] Japan road association: Road earthwork-embankment work guidelines, MARUZEN publishing, 2010, pp.1-310.

[13] Honda M., Iizuka A., Ohno S., Kawai K. and Wang W.: A study of the evaluation method for deformation characteristic of compacted soil, journal of JSCE, No806/III-73, 2005, pp.33-44.

[14] Mualem, Y.: A new model for predicting the hydraulic conductivity of unsaturated porous media, Water Resources Research, Vol.12, No.3, 1976, pp.514-522.

[15] Cabinet office, Government of Japan: About the damage situation related to Typhoon No. 19 etc. in the first year of Reiwa, 2020, pp.1-116.